

Crowding of interacting fluid particles in porous media through molecular dynamics: breakdown of universality for soft interactions

Simon K. Schnyder^{1,2,*} and Jürgen Horbach^{2,†}

¹*Fukui Institute for Fundamental Chemistry, Kyoto University, Kyoto 606-8103, Japan*

²*Institut für Theoretische Physik II, Heinrich-Heine-Universität Düsseldorf, Universitätsstraße 1, 40225 Düsseldorf, Germany*

(Dated: January 27, 2018)

Molecular dynamics simulations of interacting soft disks confined in a heterogeneous quenched matrix of soft obstacles show dynamics which is fundamentally different from that of hard disks. The interactions between the disks can enhance transport when their density is increased, as disks cooperatively help each other over the finite energy barriers in the matrix. The system exhibits a transition from a diffusive to a localized state but the transition is strongly rounded. Effective exponents in the mean-squared displacement can be observed over three decades in time but depend on the density of the disks and do not correspond to asymptotic behavior in the vicinity of a critical point, thus showing that it is incorrect to relate them to the critical exponents in the Lorentz model scenario. The soft interactions are therefore responsible for a breakdown of the universality of the dynamics.

The transport of matter in heterogeneous porous materials is widespread, e.g. crowding phenomena in biology [1–6], ion-conduction in silicate glasses [7, 8], hydrology [9, 10], and other situations [11–15]. Such systems consist of at least two components, characterised by a strong separation of time scales. The more mobile component often exhibits anomalous diffusion, i.e. its mean-squared displacement $\delta r^2(t)$ grows nonlinearly over long periods of time. Often, anomalous diffusion can be characterised by an effective exponent, $\delta r^2(t) \sim t^x$ with typically $x < 1$, with a wide range of values for x found. It remains unclear if the observed exponents merely represent transient behavior or whether they can be connected to a universal behavior with a well-defined exponent. This question will be addressed here.

A paradigm for the modeling of transport in heterogeneous media is the Lorentz Model (LM) [16–23], where anomalous diffusion arises as a universal long-time limit: In its simplest version, a single mobile particle moves in the static void space formed by overlapping hard disk obstacles. At low obstacle density, the mobile particle freely explores the system and exhibits regular diffusion. At high densities, it becomes trapped in finite pockets of obstacles. In-between there is a localization transition, where the void space of the system stops to percolate, the system becomes self-similar, and anomalous diffusion occurs. This transition is a dynamic critical phenomenon and the exponent of the anomalous diffusion is universal [2, 14].

The LM can be generalized by introducing interacting mobile particles and soft instead of hard interactions, making it more comparable to realistic porous materials. But how such generalizations change the dynamics is not well understood. An extension [24–27] of the mode coupling theory of the glass transition (MCT) [28] predicts the LM localization transition to persist for interacting fluids in porous media, i.e. that the nature of the transition is unchanged by the interactions, and that the critical behavior is qualitatively the same. Evidence from simulations of model porous media with interacting particles both with hard and soft interactions has been inconclusive [29–34]. While a localization transition and ex-

tended anomalous diffusion are observed, the exponents seldomly match the predictions. Still, so far it seemed to be evident that porous media with soft or hard potentials are qualitatively equivalent, even though energy barriers in systems with soft potentials are finite and therefore are crossable by soft particles [35–37].

Here, we perform molecular dynamics simulations of interacting soft disks confined in a soft heterogeneous matrix of obstacles. By systematically moving away from the single-particle case, we investigate how interactions between the mobile particles influence the dynamics. With increasing obstacle density the system exhibits a gradual transition from delocalized to localized dynamics. Subdiffusion with constant exponents can be identified for up to three decades in time. However, our results show that the system exhibits fundamentally different dynamics from the LM. Whereas for the single-particle case a mapping onto the LM transition is possible [36], we find here that the universality of the dynamics breaks down. The interaction of particles with each other makes each particle’s energy time-dependent; the free area available to it changes with each collision with other mobile particles. In that sense, the free volume in soft systems is dynamic – not static as in the LM – with drastic consequences. Mobile particles help each other over potential barriers, speeding up the dynamics when the mobile particle density is increased. This is impossible for interacting hard disks, thus giving a rare example where *soft and hard interactions are qualitatively different*. Even though exponents similar to the LM exponent may occur, we show that they merely represent *effective, non-universal* exponents which are highly tunable via the particle interactions. Thus they should not be linked to the anomalous exponent of the LM. In experiments, where interactions are typically quite complex, the LM can therefore at best serve as a tool for qualitative interpretation.

Simulation details Matrix (index M) and fluid particles (F) interact via a smoothly truncated, purely repulsive Weeks-Chandler-Andersen (WCA) potential [38], i.e. a Lennard-Jones potential which is truncated in the minimum and shifted. The size of fluid and matrix particles is given by σ_F and σ_M .

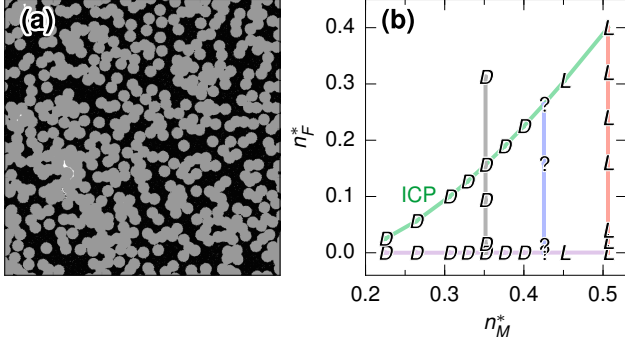


Figure 1. *Simulation snapshots and state diagram.* (a) All positions of the fluid particles over one simulation run at $n_M^* = 0.33$ and $n_F^* = 0.127$ shown as black dots. Obstacles shown in grey. (b) State diagram of the system with D marking diffusive, L marking effectively localized states, and $?$ marking states where the dynamic state was unclear on the time scale of the simulation. The path crossing the critical point at finite n_F^* is denoted ICP (Interacting-particles Critical Path).

The matrix structures are obtained as snapshots of equilibrated liquids. For ensemble averaging, we use 100 statistically independent matrix structures with up to $N_M = 16\,000$ particles each at number density $n_M := N_M/L^2 = 0.278 (\sigma_M)^{-2}$, corresponding to system sizes of up to $L/\sigma_M = 240$. The energy coefficient for the interactions between matrix particles ε_M sets the simulation's energy unit. For more details, Ref. [36]. Fluid particles are inserted into the frozen matrix with number density $n_F := N_F/L^2$, Fig. 1(a). Fluid particles interact with matrix particles with coefficients $0.1\varepsilon_M$ and $(\sigma_M + \sigma_F)/2 =: \sigma$. For the interaction between fluid particles, we use ε_M . Newton's equations of motion are integrated with the velocity-Verlet algorithm [39] with time step $7.2 \cdot 10^{-4}t_0$ with $t_0 := [m(\sigma_M)^2/\varepsilon_M]^{1/2}$ and $m = 1.0$ the mass of a fluid particle. The fluid particles are equilibrated using a simplified Andersen thermostat [40] by randomly drawing their velocities from a Maxwell distribution every 100 steps for up to $1.4 \cdot 10^5 t_0$. Up to 2400 fluid particles per host structure are used for runs of up to nearly $10^6 t_0$. For the calculation of time averages, 10 time origins per run are used, spaced equidistantly over the whole simulation time.

We use two control parameters: The interaction range between matrix and fluid particles $\sigma := (\sigma_F + \sigma_M)/2$ is tuned by the *diameter of the fluid particles* σ_F . This defines the reduced number density $n_M^* := n_M \sigma^2$ of the matrix. In addition, we vary the *number density of fluid particles* n_F by inserting more or fewer particles into the matrix. Both n_F and σ_F change the reduced number density $n_F^* := n_F \sigma_F^2$ of the fluid. The control parameters map out the state diagram of n_F^* and n_M^* , see Fig. 1(b). To determine the dynamic state of the systems, the mean-squared displacement (MSD) $\delta r^2(t) = \langle |\vec{r}(t) - \vec{r}(0)|^2 \rangle$ was calculated from the particle positions $\vec{r}(t)$ as a time- and ensemble average. The systems where the MSD became diffusive, i.e. $\delta r^2(t) \sim 4Dt$ with diffusion coefficient D for $t < 7 \cdot 10^5$, are marked delocalized,

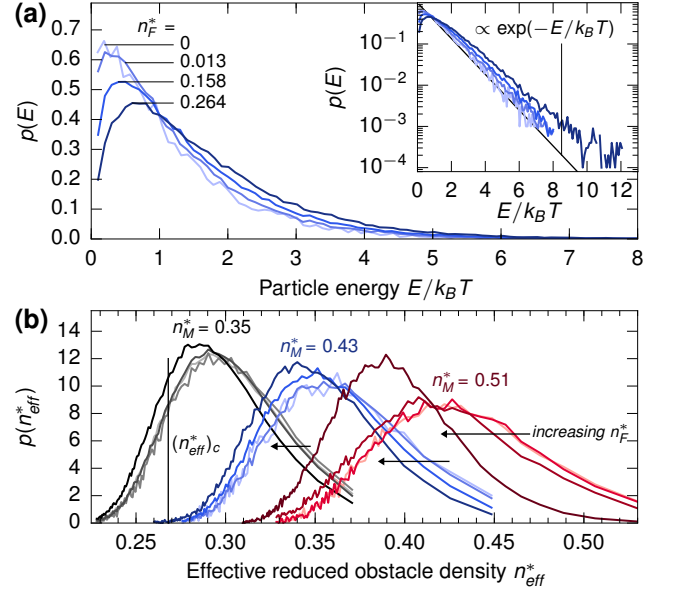


Figure 2. *Energy and density distributions.* (a) Energy distributions $p(E)$ of the fluid particles for $n_M^* = 0.43$ and a range of n_F^* . Inset: same data in semilog. plot. (b) Effective reduced obstacle density distribution $p(n_{\text{eff}}^*)$ calculated from $p(E)$ for $n_M^* = 0.35, 0.43$ and 0.51 and fluid densities $n_F^* = 0, 0.016, 0.094, 0.313, n_F^* = 0, 0.013, 0.158, 0.264$, and $n_F^* = 0, 0.020, 0.160, 0.400$ respectively. Darker colors indicate higher n_F^* . The critical effective density is $(n_{\text{eff}}^*)_c \approx 0.268$ [36].

“ D ”; states where the MSD converged to a finite long-time limit are marked localized, “ L ”. The remaining points are marked as “?”. We discuss the dynamics along the marked paths. The path along $n_F^* = 0$ represents the ideal gas limit of non-interacting tracers, for which the rounding of the transition was discussed recently [36]. Starting from this confined ideal gas, n_F^* was gradually increased for constant n_M^* to study the modification of the dynamics by the interaction between fluid particles. To study delocalized dynamics, the dynamics close to the localization transition, and localized dynamics, respectively, we chose densities $n_M^* = 0.35, 0.43$, and 0.51 .

Effective matrix density distributions If the energy E of a tracer is conserved, an effective hard-disk interaction diameter $\sigma_{\text{eff}}(E, \sigma)$ can be calculated, mapping the system onto an effective LM with matrix density $n_{\text{eff}}^* := n_M (\sigma_{\text{eff}})^2$ [36]. But here the particles interact, exchange energy, and have a time-dependent σ_{eff} . While mapping a single tracer's dynamics onto the LM is impossible, the time-independent probability distribution $p(n_{\text{eff}}^*)$ for the whole system *can* be calculated. With the energy of a tracer j ,

$$E_j = \frac{m\vec{v}_j^2}{2} + \sum_{k \in M} V_{MF}(|\vec{r}_j - \vec{r}_k|) + \frac{1}{2} \sum_{\substack{k \neq j, \\ k \in F}} V_{FF}(|\vec{r}_j - \vec{r}_k|).$$

the single-particle energy distribution $p(E)$ can be calculated from the simulation as the histogram of tracer energy, Fig. 2(a)

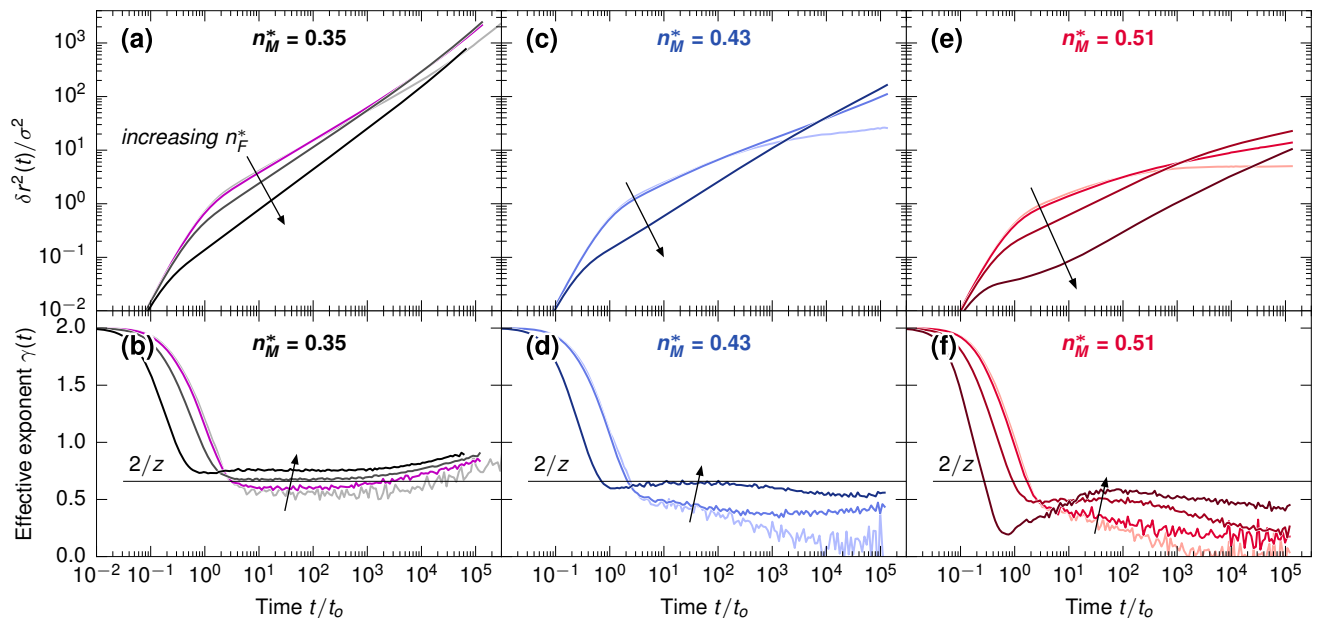


Figure 3. *Anomalous transport.* Mean-squared displacements $\delta r^2(t)$ and effective exponents $\gamma(t)$ for $n_M^* = 0.35, 0.43$, and 0.51 . Fluid densities are $n_F^* = 0, 0.016, 0.094, 0.313$ for (a, b) ($n_F^* = 0.016$ in purple for clarity); $n_F^* = 0, 0.013, 0.264$ for (c, d); and $n_F^* = 0, 0.020, 0.160, 0.400$ for (e, f). In (b, d, f), the critical exponent of the two-dimensional LM $2/z = 2/3.036$ [21] shown as black line.

for $n_M^* = 0.43$. The distributions have a peak at small energies which decreases with increasing n_F^* . The high-energy tail becomes more pronounced with increasing n_F^* but always decays exponentially, see inset. The same holds for $n_M^* = 0.35$ and 0.51 (not shown here). From $p(E)$ the effective density distribution $p(n_{\text{eff}}^*)$ was calculated, see Ref. 36 and Fig. 2(b). Large E map onto small σ_{eff} . In the effective hard-disk system, the matrix ceases to percolate at critical density $(n_{\text{eff}}^*)_c$. $n_{\text{eff}}^* < (n_{\text{eff}}^*)_c$ correspond to delocalized and $n_{\text{eff}}^* > (n_{\text{eff}}^*)_c$ to localized states. The broad obstacle density distributions are indicators of strongly averaged dynamics.

The distributions $p(n^*)$ for $n_M^* = 0.35$ are partly on the delocalized side. Increasing n_F^* at constant n_M^* shifts the whole distribution towards lower n_{eff}^* , indicating that on average more particles are delocalized at any given time. This also shifts the localization transition towards higher n_M^* at constant n_F^* . This generic shift of the distribution upon increasing n_F^* leads from localization to delocalization in a system close to the localization transition, e.g. at $n_M^* = 0.43$: Whereas at small densities, $n_F^* \leq 0.158$, the distribution $p(n_{\text{eff}}^*)$ is on the localized side, at $n_F^* = 0.264$, delocalized states become available. For $n_M^* = 0.51$ the distribution stays on the localized side.

Dynamics The MSD undergoes strong changes on both sides of the transition as the fluid density is increased. At $n_M^* = 0.35$ (Fig. 3(a)), all investigated systems are delocalized, as anticipated from $p(n_{\text{eff}}^*)$. The confined ideal gas ($n_F^* = 0$) shows subdiffusion on intermediate times before becoming diffusive at long times. The MSD at $n_F^* = 0.016$ (purple), while nearly unchanged at small and intermediate times, shows considerably enhanced long-time diffusion. This hap-

pens even though the energy distribution is nearly the same.

The speeding up of the dynamics stems from the *exchange* of energy between particles: When particles exchange energy, more particles have a high energy at some point during the simulation and can escape void pockets and explore more of the void space. This is only possible in systems with soft interactions, where the barriers between void pockets are finite and thus surmountable.

The MSD for $n_F^* = 0.094$ is suppressed on short and intermediate times compared to the confined ideal gas because collisions of particles with their neighbors slow down the exploration of the void volume. But at long times the MSD catches up with the MSD at $n_F^* = 0.013$ and overtakes it. At $n_F^* = 0.313$, the dynamics is further slowed down. At long times, the diffusion has slowed down compared to the systems at intermediate n_F^* but is still similar to the confined-ideal-gas case. This happens even though a larger fraction of particles is delocalized at any given time than in the less dense systems, as inferred from $p(n^*)$. This indicates competition at long times between a speeding up via energy exchange and a slowing down via caging by neighbors.

The effective exponent of the MSD $\gamma(t) := d(\log \delta r^2(t))/d(\log t)$ allows identifying regimes where the MSD follows a power-law. All systems show constant $\gamma(t)$ over about 3 decades in time, Figure 3(b), with values ranging from below the LM critical exponent $2/z = 2/3.036$ [21] for $n_F^* = 0$ to above it for denser systems. Therefore, $\gamma(t)$ can be readily tuned via the fluid density. For $n_F^* = 0.094$, $\gamma(t)$ nearly matches $2/z$ which is accidental as the system is *clearly diffusive* at long times. Observing a $\gamma(t)$ close to the LM value is thus not enough to determine that a

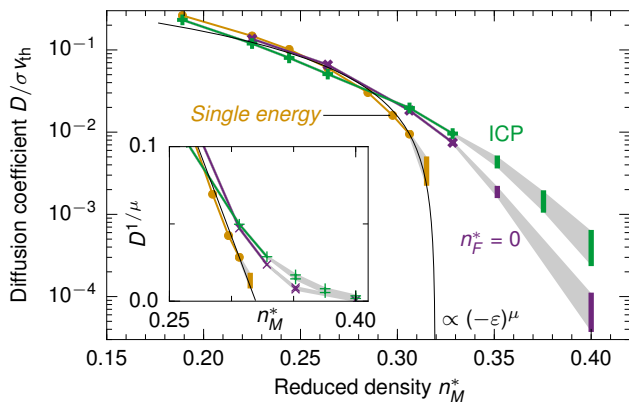


Figure 4. *Rounding of the localisation transition.* Diffusion coefficient D as function of n_M^* for the single-energy case, for $n_F^* = 0$, and for $n_F = 0.625$ (ICP in Fig. 1). Connected symbols are directly obtained from the MSD, while error bars are obtained in finite size analysis, see ref. 36. The solid line $\propto (-\varepsilon)^\mu$ with $\varepsilon = (n^* - n_c^*)/n_c^*$, critical point $n_c^* = 0.32$, and conductivity exponent $\mu = 1.309$ of the LM, serves as guide to the eye. Inset: rectification plot of same data.

system is near-critical.

For the localized system at $n_M^* = 0.51$ a similar modification of the dynamics is found (Fig. 3(e)). At $n_F^* = 0$ the MSD converges to a finite long time limit, which is a measure of the localization length. Increasing the density to $n_F^* = 0.020$ leaves the dynamics on short and intermediate times unchanged but strongly increases the long time limit, due to particles pushing each other out of void pockets (observed in trajectories). The increase of the long-time limit is evident even though the MSD does not fully converge during the simulation. All this occurs without a significant change in $p(n_{\text{eff}}^*)$. Increasing n_F^* further leads to a slowing down of the dynamics on intermediate time scales and first to a speeding up and then a slowing down at long times.

The system at $n_M^* = 0.43$ is an intermediate case, Fig. 3(c,d). At $n_F^* = 0$, the system is localized since $\gamma(t)$ decays to near 0. The corresponding distribution $p(n_{\text{eff}}^*)$ implies that all particles are localized, with a few being very close to the transition. As a result, the MSD grows slightly at all times. At higher n_F^* the localization length grows while the intermediate-time dynamics slows down. As the MSDs are not diffusive on the time scale of the simulation it is impossible to tell whether the systems at finite n_F^* are delocalized. Still, diffusion of the MSD is anticipated from the upward bend in the effective exponent $\gamma(t)$ at long times, Fig. 3(d), and the shift of $p(n_{\text{eff}}^*)$ over the critical point, Fig. 2(b).

The scaling properties of the dynamics near the localization transition were tested by crossing the transition along a path with constant $n_F = 0.625$ while varying n_M^* . Along this path, n_F^* is high enough so that the dynamics is considerably modified by the interactions. The diffusion coefficient D is similar to that of the confined ideal gas ($n_F^* = 0$), and does not follow the LM critical scaling, Fig. 4. This is in sharp contrast to

the case where the tracers of the confined ideal gas are all set to the same energy, for which said scaling has been identified [36]. The rounding of the transition is even more clearly visible in the rectification plot in the inset of Fig. 4, where data obeying the critical asymptote would fall on a straight line.

Discussion Similar to the hard-disk Lorentz model, the particles show a localization transition as well as subdiffusion in the mean-squared displacement, extending up to 3 decades in time. The associated effective exponents are tunable via the particle interactions and may even match the Lorentz model value (cf. the finding in Ref. [32]). However, whereas interacting soft-disks can push each other out of void pockets over barriers in this soft version of the Lorentz model, the situation is markedly different in the corresponding hard-disk model where the barriers, formed by closed pockets of hard obstacles, are always infinite. In the hard-disk case, localization transitions similar to those in the “original” Lorentz model with a single tracer particle can be expected and they have in fact been observed in simulations [29–31].

The tune-ability of the exponents and the speeding up of the dynamics indicate the breaking of universality. Interestingly, similar speeding up of the dynamics was observed for a binary mixture of colloids [41], where however varying the density of the more mobile component influences the structure of the less mobile component. Similarly, in a recent study of the MCT of fluids in random potential landscapes [15], a qualitatively similar speed-up was reported, as well. However, the theory still predicts a sharp localisation transition.

Our work demonstrates that the wide range of exponents seen, e.g. in crowding experiments of cellular fluids is *most likely a result of the soft interactions between the components of those systems*. One expects therefore that crowding phenomena in cells cannot in general be associated with universal anomalous diffusion.

We acknowledge financial support by the DFG Research Unit FOR1394 “Nonlinear Response to Probe Vitrification” (HO 2231/7-2, project P8).

* skschnyder@gmail.com

† horbach@thphy.uni-duesseldorf.de

- [1] M. Weiss, in *New Models of the Cell Nucleus: Crowding, Entropic Forces, Phase Separation, and Fractals*, edited by R. Hancock and K. W. Jeon (Academic Press, 2014), vol. 307 of *Int. Rev. Cell Mol. Biol.*, chap. 11, pp. 383–417.
- [2] F. Höfling and T. Franosch, *Rep. Prog. Phys.* **76**, 046602 (2013).
- [3] I. M. Sokolov, *Soft Matter* **8**, 9043 (2012).
- [4] M. J. Saxton, *Biophysical Journal* **103**, 2411 (2012).
- [5] H. Berry and H. Chat, *Phys. Rev. E* **89**, 022708 (2014).
- [6] B. Sung and A. Yethiraj, *Phys. Rev. Lett.* **96**, 228103 (2006).
- [7] A. Bunde, *Solid State Ionics* **105**, 1 (1998).
- [8] J. Horbach, W. Kob, and K. Binder, *Phys. Rev. Lett.* **88**, 125502 (2002).
- [9] B. Bijeljic, P. Mostaghimi, and M. J. Blunt, *Phys. Rev. Lett.* **107**, 204502 (2011).
- [10] P. K. Kang, S. Brown, and R. Juanes, *Earth Planet. Sci. Lett.*

- 454**, 46 (2016).
- [11] H. Gleiter, *Acta Mater.* **48**, 1 (2000).
- [12] H. Brenner and D. Edwards, *Macrotransport Processes*, Butterworth-Heinemann series in chemical engineering (Butterworth-Heinemann, 1993), ISBN 9780750693325.
- [13] O. Bénichou, C. Chevalier, J. Klafter, B. Meyer, and R. Voituriez, *Nat Chem* **2**, 472 (2010).
- [14] D. Ben-Avraham and S. Havlin, *Diffusion and Reactions in Fractals and Disordered Systems* (Cambridge University Press, Cambridge, 2000), 1st ed.
- [15] T. Konincks and V. Krakoviack, *Soft Matter* **13**, 5283 (2017).
- [16] H. Lorentz, *Proc. R. Acad. Sci. Amsterdam* **7**, 438 (1905).
- [17] H. V. Beijeren, *Rev. Mod. Phys.* **54**, 195 (1982).
- [18] F. Höfling, T. Franosch, and E. Frey, *Phys. Rev. Lett.* **96**, 165901 (2006), 0510442v2.
- [19] F. Höfling and T. Franosch, *Phys. Rev. Lett.* **98**, 140601 (2007).
- [20] F. Höfling, T. Munk, E. Frey, and T. Franosch, *J. Chem. Phys.* **128**, 164517 (2008).
- [21] T. Bauer, F. Höfling, T. Munk, E. Frey, and T. Franosch, *Eur. Phys. J.-Spec. Top.* **189**, 103 (2010).
- [22] M. Spanner, F. Höfling, S. C. Kapfer, K. R. Mecke, G. E. Schröder-Turk, and T. Franosch, *Phys. Rev. Lett.* **116**, 060601 (2016), 1601.06091.
- [23] Y. Jin and P. Charbonneau, *Phys. Rev. E* **91**, 042313 (2015).
- [24] V. Krakoviack, *Phys. Rev. Lett.* **94**, 065703 (2005).
- [25] V. Krakoviack, *Phys. Rev. E* **75**, 031503 (2007).
- [26] V. Krakoviack, *Phys. Rev. E* **79**, 1 (2009).
- [27] V. Krakoviack, *Phys. Rev. E* **84**, 050501 (2011).
- [28] W. Götze, *Complex Dynamics of Glass-Forming Liquids: A Mode-Coupling Theory (International Series of Monographs on Physics)*, vol. 143 (Oxford University Press, 2009), ISBN 9780199235346.
- [29] J. Kurzidim, D. Coslovich, and G. Kahl, *Phys. Rev. Lett.* **103**, 138303 (2009).
- [30] J. Kurzidim, D. Coslovich, and G. Kahl, *Phys. Rev. E* **82**, 041505 (2010).
- [31] J. Kurzidim, D. Coslovich, and G. Kahl, *J. Phys. Condens. Matter* **23**, 234122 (2011).
- [32] K. Kim, K. Miyazaki, and S. Saito, *Europhys. Lett.* **88**, 36002 (2009).
- [33] K. Kim, K. Miyazaki, and S. Saito, *Eur. Phys. J.-Spec. Top.* **189**, 135 (2010).
- [34] K. Kim, K. Miyazaki, and S. Saito, *J. Phys. Condens. Matter* **23**, 234123 (2011).
- [35] T. O. E. Skinner, S. K. Schnyder, D. G. A. L. Aarts, J. Horbach, and R. P. A. Dullens, *Phys. Rev. Lett.* **111**, 128301 (2013).
- [36] S. K. Schnyder, M. Spanner, F. Höfling, T. Franosch, and J. Horbach, *Soft Matter* **11**, 701 (2015).
- [37] S. K. Schnyder, T. O. E. Skinner, A. L. Thorneywork, D. G. A. L. Aarts, J. Horbach, and R. P. A. Dullens, *Phys. Rev. E* **95**, 032602 (2017).
- [38] J. D. Weeks, D. Chandler, and H. C. Andersen, *J. Chem. Phys.* **54**, 5237 (1971).
- [39] K. Binder, J. Horbach, W. Kob, W. Paul, and F. Varnik, *J. Phys. Condens. Matter* **16**, 429 (2004).
- [40] H. C. Andersen, *J. Chem. Phys.* **72**, 2384 (1980).
- [41] Th. Voigtmann and J. Horbach, *Phys. Rev. Lett.* **103**, 205901 (2009).